- 1 (Draft)

CONF-811150--1 Draft

DE82 004113

81-271

NOTE: This is a draft of paper being submitted for publication. Contents of the paper should not be quoted nor referred to without permission of the authors.

[To be published in the Proceedings of the Yamada Conference on Point Defects and Defect Interactions in Metals, November 16-20, 1981, Kyoto, Japan]

VACANCY AND INTERSTITIAL LOOPS IN IRRADIATED COPPER

B. C. Larson and F. W. Young, Jr.

SOLID STATE DIVISION
OAK RIDGE NATIONAL LABORATORY
Operated by
UNION CARBIDE CORPORATION
for the
UNITED STATES DEPARTMENT OF ENERGY
Oak Ridge, Tennessee

November 1981

MSW

Vacancy and Interstitial Loops in Irradiated Copper*

B. C. Larson and F. W. Young, Jr.

Solid State Division, Oak Ridge National Laboratory, Oak Ridge, TN 37830

Significant advances have been made in diffuse scattering studies of irradiation induced dislocation loops in metals. Numerical calculational procedures have been developed that provide accurate diffuse scattering cross sections for vacancy and interstitial loops, and these cross sections have been used in conjunction with x-ray diffuse scattering studies of neutron and ion irradiated copper. Size distributions and concentrations have been obtained for both vacancy and interstitial loops and these results are compared with electron microscopy measurements. The size distributions obtained from diffuse scattering measurements show the vacancy loops to be smaller and more numerous than the interstitial loops, and indicate that equal numbers of vacancies and interstitials are in loops. The diffuse scattering and microscopy size distributions agree at the larger sizes, but the diffuse scattering method identifies more loops of the smaller sizes.

I. INTRODUCTION

The clustering of point defects into dislocation loops is one of the principle mechanisms whereby radiation damage is retained in metals during irradiation at temperatures above stage III, or after annealing following low temperature irradiations. The presence of such loops has been well established by electron microscope investigations [1,2], and vacancy loops in particular have been established as playing an important role in the process of void formation [3] during elevated temperature irradiations. The mechanism of radiation enhanced creep [4] is also thought to involve the formation and growth of dislocation loops from point defects. Hence, the characterization and understanding of the processes involved in the formation and growth of dislocation loops in metals is of significant importance in the understanding of radiation effects in metals.

Electron microscopy investigations have shown that both vacancy and interstitial loops exist in metals irradiated at (or irradiated and annealed to) temperatures above stage III. These investigations have measured dislocation loop size distributions and concentrations as a function of irradiation (neutron, electron, ion) dose and temperature in a variety of metals. Making use of the ability to distinguish between vacancy and interstitial loops, TEM observations on radiation induced defects have shown interstitial loops to be larger than vacancy loops; however, it is not unusual to find the total area of interstitial loops identified to exceed [5,6] the area of vacancy loops by substantial margins, although some reports show nearly equal areas [1].

X-ray diffuse scattering measurements of size distributions of dislocation loops in irradiated metals [7,8] have been found to be in substantial agreement with TEM observations, except for the number of small (< 30 Å diameter) loops. X-ray

*Research sponsored by the Division of Materials Sciences, U.S. Department of Energy under contract W-7405-eng-26 with Union Carbide Corporation.

measurements have consistantly reported significantly more defects in the < 30 Å diameter range. With the availability [9,10] of more precise diffuse scattering cross sections and improvements in measuring techniques, it has now become possible to carry out detailed size distribution analyses for both vacancy and interstitial loops using x-ray diffuse scattering. This paper reports the use of x-ray diffuse scattering for detailed studies of vacancy and interstitial loops in neutron and Ni ion irradiated copper.

II. THEORY

In the single defect approximation, the scattering cross section for randomly distributed defects in a crystal lattice is given by [9]

$$\frac{d\sigma(\vec{K})}{d\Omega} = (r_e F)^2 \mid A(\vec{K}) \mid^2 , \tag{1}$$

where the scattering vector $\vec{K} = \vec{h} + \vec{q}$ specifies the measuring position in terms of the reciprocal lattice vector $\vec{h}$ and a vector $\vec{q}$ relative to $\vec{h}$. r_e is the classical electron radius, F is the scattering factor for a unit cell of the crystal lattice and $A(\vec{K})$ is the scattering amplitude associated with the defect. For dislocation loops, $A(\vec{K})$ contains contributions from the lattice distortions surrounding the loop as well as from the atoms comprising the dislocation loop, and can be written as [9,10,11]

$$A(\vec{K}) = \sum_i e^{i\vec{K}\cdot\vec{r}_i^L} + \sum_j e^{i\vec{q}\cdot\vec{r}_j} \left(e^{i\vec{K}\cdot\vec{S}_j} - 1\right) . \tag{2}$$

In this expression the first term represents the direct or Laue scattering from loop atoms at positions $\vec{r}_i^L$, and the second term represents the scattering amplitude associated with the displacements $\vec{S}_j$ of the surrounding atoms from their regular lattice positions $\vec{r}_j$.

For evaluation purposes, the distortion scattering is separated into the Huang scattering ($i\vec{K}\cdot\vec{S}$), generated by the long range displacement fields, and the asymptotic scattering arising from the larger displacements close to the dislocation loop. This can be written as

$$A(\vec{K}) = \sum_i e^{i\vec{K}\cdot\vec{r}_i^L} + i\vec{K}\cdot\vec{S}(\vec{q}) + \sum_j e^{i\vec{q}\cdot\vec{r}_j} \left(e^{i\vec{K}\cdot\vec{S}_j} - 1 - i\vec{K}\cdot\vec{S}_j\right) , \tag{3}$$

where $\vec{S}(\vec{q})$ is the Fourier transformed displacement field. This form has the advantage that $i\vec{K}\cdot\vec{S}$ can be evaluated analytically [9,10,11] through the Fourier transformed Green's function and the double force tensor of the loop, while the remaining part of the distortion scattering has only short range displacement field contributions that can be readily evaluated numerically. Inserting Eq. (3) into Eq. (1) for loops of radius R leads to the characteristic form of the Huang scattering for $q \ll 1/R$ of

$$\frac{d\sigma(\vec{K})}{d\Omega} \sim \frac{K^2 b^2 R^4}{q^2} . \tag{4}$$

For $q > 1/R$ the intensity decreases roughly as $1/q^4$, and this scattering is referred to as the asymptotic (or Stokes-Wilson) scattering and has the form

$$\frac{d\sigma(\vec{K})}{d\Omega} \sim \frac{KbR^2}{q^4} . \tag{5}$$

The Huang scattering has been used [12] very effectively in the study of defects and defect symmetry; however, for the study of size distributions and concentrations of vacancy and interstitial loops, it is more convenient to use the asymptotic scattering [10] because it measures the second (R^2) moment of the size distribution rather than the fourth (R^4) moment, and because it is sensitive to the sign of the

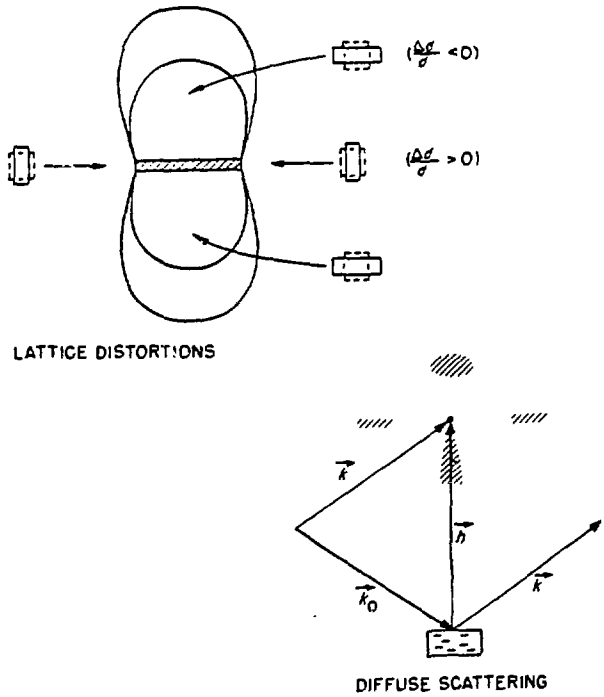

Fig. 1. Schematic view of lattice distortions for an interstitial loop and the asymptotic diffuse scattering scaled by q^4.

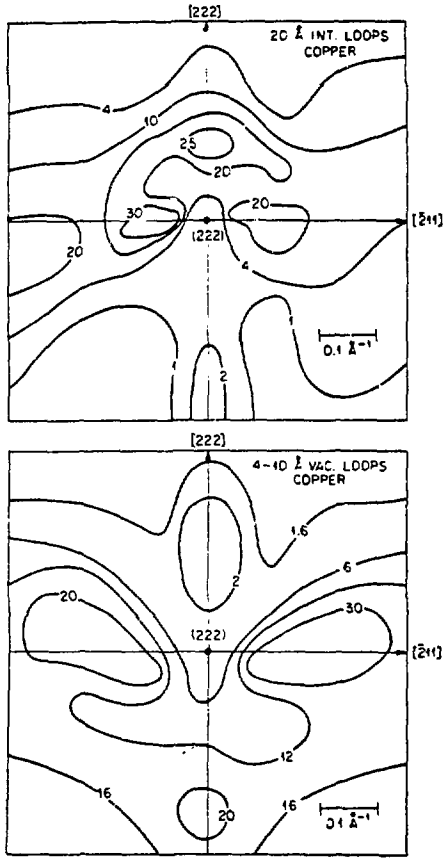

Fig. 2. Calculated scattering for 20 Å interstitial and four 10 Å vacancy loops (scaled by q^4).

Burgers vector (i.e., vacancy or interstitial type). This scattering [13] is comprised of local Bragg-like scattering from the compressed (interstitial) or expanded (vacancy) regions near the loop planes. In this region the strain is surprisingly constant [10] and is given by $\Delta d/d \simeq -b/4R$; therefore, the scattering intensity will be enhanced at $q \simeq bh/4R$ for the case of loops oriented normal to $\vec{h}$. Although the intensity enhancement is masked to some extent by the $1/q^4$ falloff of the intensity, the enhancement can be observed by scaling the scattering by q^4. This effect is depicted schematically in Fig. 1 where the lattice displacement contours and the sense of lattice strain ($\Delta d/d$) are shown for an interstitial loop. The scattering enhancements expected (after scaling by q^4) are shown in the lower part of the figure. Regions with $\Delta d/d < 0$ contribute to the hatched area above the Bragg point while regions with $\Delta d/d > 0$ contribute to weak scattering in the rather elongated hatched region below the Bragg point. The ridges of scattering shown on both the right and left side of the Bragg point are expected as a result of essentially dilation free, rotational strains found in the regions between $\Delta d/d > 0$ and $\Delta d/d < 0$. Of course, for vacancy loops the scattering above and below the Bragg point will interchange positions, thereby providing a basis for distinguishing between vacancy and interstitial loops. As pointed out above, the position of the intensity peak above (or below) the Bragg point is given by $q \simeq bh/4R$ and therefore makes size determinations as well as type determinations possible through this scattering.

The above (semi-quantitative) picture has been constructed with the aid of detailed diffuse scattering calculations [9,10] utilizing Eq. (3) and numerically calculated [14] displacement fields. Examples of such calculations are shown in Fig. 2, where scattering contours are shown for {111} interstitial and vacancy loops in

copper with a/3<111> Burgers vectors. These calculations are averaged for all {111} orientations and correspond to scattering near the 222 reflection. These calculations have been scaled by q^4 so that they show the same features sketched in Fig. 1. They emphasize the nearly ten-fold higher scattering at positive q for interstitial loops and the corresponding increase at negative q for vacancy loops. The inverse R dependence of the position of the peak is also demonstrated, as the intensity peak is a factor of two further from the origin for 10 Å vacancy loops than for the 20 Å interstitial loops. That the combined scattering of four 10 Å vacancy loops has a peak scattering essentially the same as that for one 20 Å loop emphasizes the fact that the asymptotic region is proportional to the second moment (R^2) and therefore gives equal scattering weight to clusters with equal numbers of point defects, independent of their sizes. The intensity peaks to the right and left of the Bragg point are rather high, but since they are not particularly sensitive to the type of loop, they are not as useful a diagnostic tool as the intensity modulations along the [111] direction.

The experimentally measured intensity for a thick sample with homogeneously distributed defects (in the symmetric scattering geometry) is related to these scattering cross sections through

$$I(\vec{K}) = \frac{I_o}{\sin\Theta} \sum_i C_i \frac{d\sigma_i(\vec{K})}{d\Omega} \Delta\Omega \int_o^\infty e^{2\mu_o t/\sin\Theta}\, dt \qquad (6)$$

$$= \frac{I_o}{2\mu_o} \sum_i C_i \frac{d\sigma_i(\vec{K})}{d\Omega} \Delta\Omega \ . \qquad (7)$$

In this expression I_o is the incident beam power, μ_o is the linear absorption coefficient, Θ is the angle of the incident (and scattered) x-ray beams with the crystal surface, C_i is the volume concentration of loops of radius R_i with scattering cross section $d\sigma_i/d\Omega$ and $\Delta\Omega$ is the solid angle subtended by the detector. For the case of a nonhomogeneous (depth) distribution, Eq. (7) may be written in the form of

$$I(\vec{K}) = \frac{I_o}{\sin\Theta} \sum_i C_i^o \frac{d\sigma_i(\vec{K})}{d\Omega} \Delta\Omega \int_o^\infty \frac{C_i(t)}{C_i^o} e^{-2\mu_o t/\sin\Theta}\, dt \ , \qquad (8)$$

where t is the depth into the crystal, and $C_i(t)$ and C_i^o are the loop concentrations as a function of depth and at some reference point (say at the surface or at a depth of particular interest), respectively. Under conditions where the size distribution may be assumed to be constant with depth, and where the relative shape of the concentration profile can be specified, the concentration and size distribution, $C_i(t)$, at any depth can be determined using Eq. (8).

III. EXPERIMENT

In this study, we have used dislocation free copper crystals with <111> orientations to study neutron and heavy ion irradiation induced dislocation loops in copper. The neutron irradiation was carried out at liquid helium temperatures [15] (1.3×10^{18} n/cm^2) and the samples were warmed to room temperature before measuring. The ion irradiation was 60 MeV Ni ion irradiation [8] at room temperature for a dose of 1.3×10^{13} Ni ions/cm^2. The x-ray measurements were made at 10 K to minimize thermal diffuse scattering, and the thermal scattering, the scattering from the Bragg tails, and the Compton scattering were all removed through measurements on unirradiated crystals. A 12 Kw rotating anode CuKα x-ray source was used in connection with a linear, position sensitive detector. The experimental scattering geometry is shown in Fig. 3, where it can be seen that changing the sample angle makes it possible to make measurements over a plane near the reciprocal lattice point. Measurements were made along the [111] direction by choosing the point where the Ewald sphere crossed the [111] direction for appropriate sample angles.

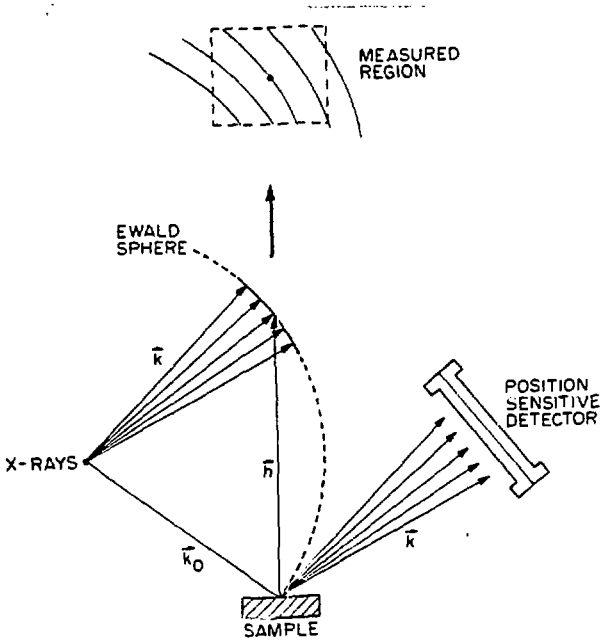

Fig. 3. Composite real and reciprocal space diagram of the diffuse scattering geometry.

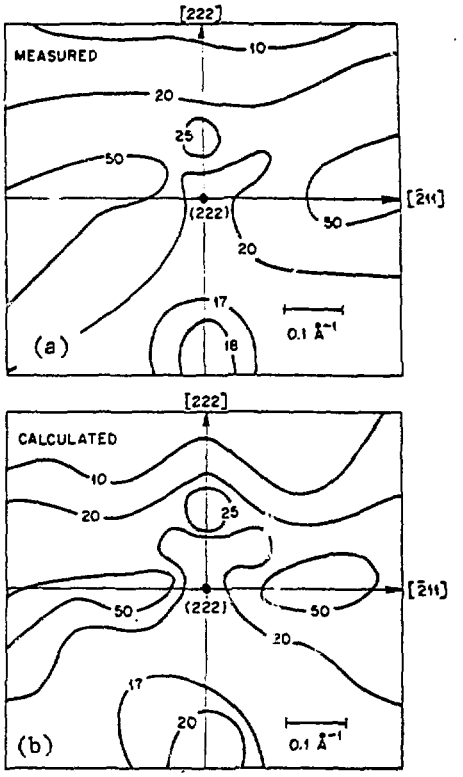

Fig. 4. Measured diffuse scattering (x q^4) from neutron irradiated copper and combined calculated scattering from Fig. 1.

IV. RESULTS

Figure 4a shows the results of x-ray diffuse scattering measurements made on 4 K neutron irradiated copper after warming to room temperature. These measurements have been scaled by q^4 for plotting (as discussed in the theory section above) so that the intensity modulations of the asymptotic region can be studied. The intensity goes to zero at the origin due to the $1/q^2$ dependence of the Huang scattering in that region. Figure 4a shows an intensity peak at both positive and negative q along the [111] direction as well as high ridges along the [$\bar{2}$11] directions. Referring back to Fig. 2, the high intensity at both positive and negative q implies that both vacancy and interstitial loops are present in the sample. In order to compare the measured scattering in Fig. 4a with the calculations in Fig. 2, the intensities in Figs. 2a,b have been superposed and plotted in Fig. 4b. The similarities in the measured and calculated contour plots indicates directly that some combination of 20 Å interstitial loops and 10 Å vacancy loops would provide a reasonable representation of the size distribution of the dislocation loops in the crystal.

Although this overall agreement between the measured and calculated results is satisfying, more detailed information has been obtained through direct fitting of the intensity along the [111] directions with calculated scattering cross section data for 10, 15, 20, 30, and 40 Å loops of both vacancy and interstitial types. The results of this fitting are shown in Fig. 5 where the concentrations have been distributed over 10 Å intervals and converted to units of loops/cm^3/Å so that the crosshatched area represents the total number of loops. We see directly that a large number of 10 Å vacancy loops are found to be present with only a few larger vacancy loops. On the other hand, the interstitial loops are found to be more or less equally split between 10 and 20 Å loops with a few larger loops as well. With the R^2 weighting of the scattering, most of the interstitial loop scattering will

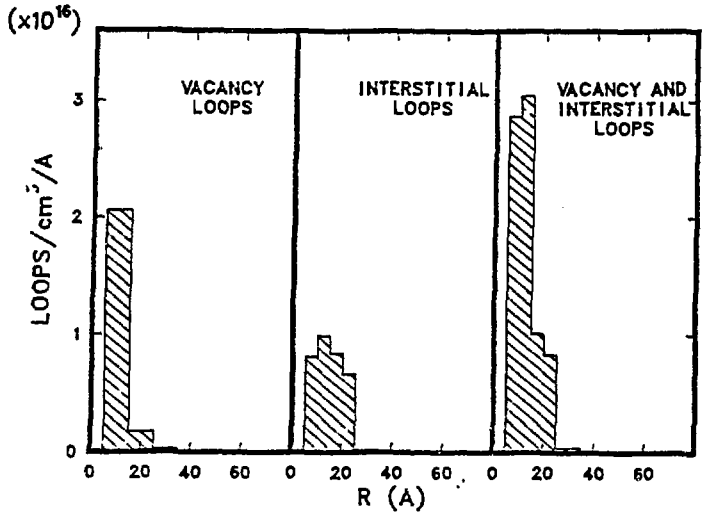

Fig. 5. Dislocation loop size distributions obtained by fitting the scattering along [111] in Fig. 4(a).

come from the 20 Å loops, so it is not surprising that a reasonable fit was obtained in Fig. 4 with only 10 Å vacancy loops and 20 Å interstitial loops. The important results here are that we can separate the size distributions of the two types of loops, that the vacancy loops are smaller than the interstitial loops, and that the total areas of the two types of loops are approximately equal (see Table I).

For the case of high energy, heavy ion damage, a similar analysis can be performed; however, the interpretation must take the depth dependence of the damage profile into account. If we make the assumption that the size distribution of the loops does not change appreciably as a function of depth, the depth dependence of the damage energy (obtained from calculations) [8] can be used as a relative measure of $C_i(t)$ in Eq. (8). It is then possible to obtain the size distribution and concentration of dislocation loops in ion irradiated materials from these x-ray measurements. Figure 6 shows x-ray scattering measurements made on copper after irradiation with 1.3×10^{13} 60 MeV Ni/cm^2 at room temperature. These data have been scaled by q^4 and represent scattering along the [111] directions. It is clear from these data that comparable numbers of vacancies and interstitials are condensed into loops in this sample, and from the positions of the peaks (smaller q for the positive direction) it may be concluded that the interstitial loops are larger, as well. The solid lines in Fig. 6 correspond to fits of scattering calculations to the measured data, and through the use of Eq. (8) and damage energy distribution calculations, we arrive at the size distributions and concentrations shown in Fig. 7 using sizes of 10, 20, 30, 40, and 60 A loops. These concentrations correspond to the depth of the damage energy peak. Again we see large numbers of small vacancy loops while the interstitials are clustered into loops of larger sizes, and of course smaller numbers. Table I shows these data in tabular form.

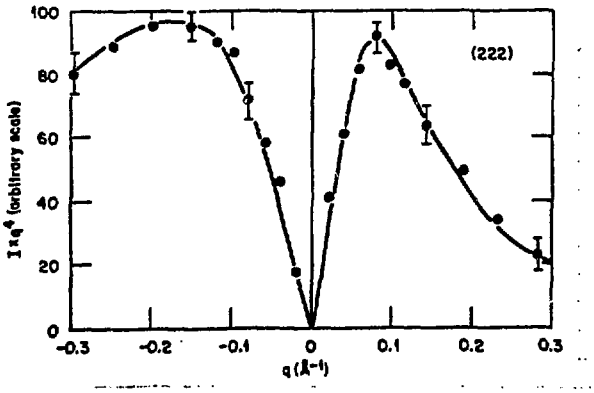

Fig. 6. Measured diffuse scattering intensity (x q^4) from Ni ion irradiated copper.

Table I. Average Loop Radii (R) and Number (N) of point defects for Interstitials (I) and Vacancies (V)

	$\langle R_I \rangle$	$\langle R_V \rangle$	N_I/N_V	N_I+N_V
1.3×10^{18} n/cm^2	14.5 Å	11.0 Å	57/43	3.9×10^{19}/cm^3
1.3×10^{13} Ni/cm^2	22.0	12.0	47/53	6.0×10^{19}

Both the neutron irradiation and the ion irradiation results yield rapidly decreasing loop concentrations with increasing size when the combined vacancy and interstitial size distributions are considered. This is reminiscent of TEM size distributions [2], and to make such a comparison more directly, Fig. 8 shows a semi-log plot of the combined size distribution from Fig. 7 together with published transmission electron microscopy measurements [8] for a similarly irradiated crystal. It is interesting to note that for sizes greater than 20 Å there is rather good agreement between the two types of measurements; however, below 20 Å the x-ray measurement indicates many more loops. It should be noted that the x-ray and TEM measurements are independent and there is no scaling involved in either data set.

V. DISCUSSION

In this work we have shown that it is possible to obtain detailed size distributions for both vacancy and interstitial loops in irradiated materials through the use of x-ray diffuse scattering. Although the electron microscopy technique has this capability as well, the diffuse scattering method is to a large extent complementary to electron microscopy. TEM can be used to image individual defects in polycrystalline as well as single crystal samples and has the capability of investigating loops in the presence of other lattice defects such as solute precipitates and voids. On the other hand, the requirements of analyzing individual defects raises problems with respect to attaining good statistical accuracy, and the tedious nature of stereo measurements, required to carry out vacancy-interstitial determinations of the loops, limits routine application of this procedure. X-ray diffuse scattering of the type used here requires single crystals and is really not applicable in cases where more than one type of defect cluster is present. However, scattering measurements possess inherently good statistical sampling and are nondestructive, so that subtle effects can be investigated and sequential measurement and treatment programs can be performed on a single sample. In addition, the diffuse scattering technique does not possess the resolution limit at small cluster sizes that is present with the electron microscope, although more severe limits exist on the concentrations that can be detected using diffuse scattering.

The comparison of an x-ray and TEM size distribution shown in Fig. 8 indicates very good agreement at the larger sizes where there can be no question of the TEM resolution, but at smaller sizes where the resolution of the microscope becomes a factor, the agreement is poor. While it cannot be established definitely that the microscope fails to image the smaller loops in this case, it must be noticed that primarily vacancy loops are present in this range (Fig. 7) and that such a large number of vacancy loops is necessary to maintain the balance of vacancies and interstitials as indicated in Table I. It should be pointed out that the discrepancy between the TEM and x-ray determined size distribution shown seems to be systematic, as similar results have been observed in a number of cases [7,8,16]. This result in connection with the observation that TEM studies of irradiation induced loops account for only a small fraction [5,6] of the vacancies in many cases, strongly suggests that the electron microscope has difficulty imaging the small vacancy clusters.

The possibility that vacancy stacking-fault tetrahedra (SFT) are present in the small sizes rather than loops has not been investigated here. Since SFT have the same volume distortion as vacancy loops with areas equal to the tetrahedra sides, it is conjectured that their scattering in the asymptotic region would be similar and could be interpreted as loop scattering. SFT scattering in the Huang region would be

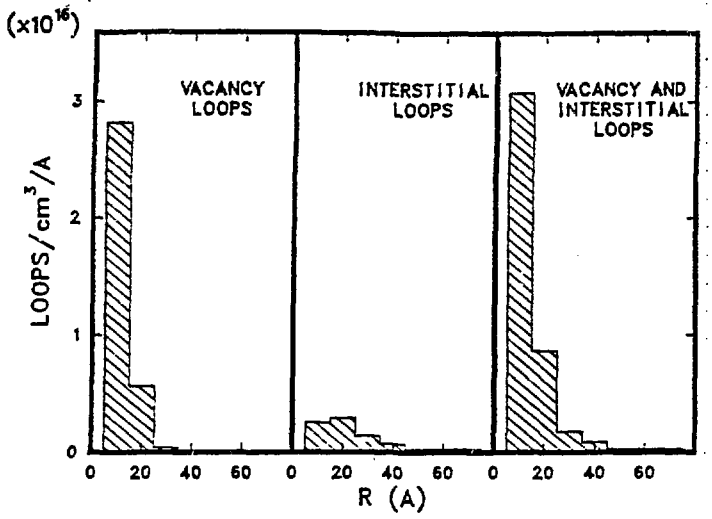

Fig. 7. Size distribution corresponding to fitting in Fig. 6.

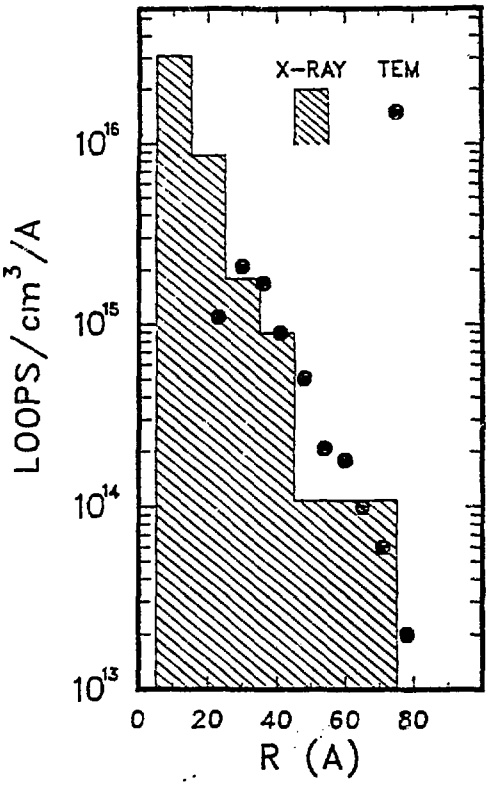

Fig. 8. Size distribution for dislocation loops in Ni ion irradiated copper determined by diffuse scattering and TEM.

different, but that has not been investigated here. However, the high intensity at negative q in Fig. 6 clearly indicates the presence of small vacancy clusters of some type.

TEM results [17] indicate that some of the larger interstitial loops in irradiated copper are unfaulted. Throughout this work we have assumed faulted loops in the fitting; however, we have inserted unfaulted loop calculations into the fitting of the larger sizes and found rather minor changes in the size distributions. This aspect will be more important in analyzing data in the larger q region where stacking-fault streak scattering is observed.

REFERENCES

1. M. Rühle, F. Häuserman and M. Rapp, Phys. Stat. Sol. 39, 609 (1970).
2. M. Rühle and J. C. Crump, Phys. Stat. Sol. (a) 2, 257 (1970).
3. A. D. Brailsford and R. Bullough, J. Nucl. Mat. 69/70, 434 (1978).
4. R. Bullough, in Fundamental Aspects of Radiation Damage in Metals, ed. by M. T. Robinson and F. W. Young, Jr., (ERDA Conf-751006-P1, Oak Ridge, Tenn., 1976), p. 1261.
5. J. Narayan and S.M. Ohr, J. Nucl. Mat. 85/86, 515 (1979).
6. A. A. Pochettino and M. Ipohorski, J. Nucl. Mat. 57, 356 (1975).
7. B. C. Larson, Ref. 4, p. 820.
8. J. B. Roberto and J. Narayan, Ref. 4, p. 120.
9. B. C. Larson and W. Schmatz, Phys. Stat. Sol. (b) 99, 267 (1980).
10. P. Ehrhart, H. Trinkaus and B. C. Larson, Phys. Rev. (Dec. 1981) in press.
11. H. Trinkaus, Phys. Stat. Sol. (b) 54, 209 (1972).
12. P. Ehrhart, J. Nucl. Mat. 69/70, 208 (1978).
13. H. Trinkaus, Z. Angew. Phys. 31, 229 (1971).
14. S. M. Ohr, Phys. Stat. Sol. (b) 64, 317 (1974).
15. Irradiation performed by T. H. Blewitt (CP-5 facility).
16. B. C. Larson, J. Appl. Cryst. 8, 150 (1975).
17. B. L. Eyre, J. Phys. F: Metal Physics 3, 497 (1973).